The Structure of the Complex of Calmodulin with KAR-2

A NOVEL MODE OF BINDING EXPLAINS THE UNIQUE PHARMACOLOGY OF THE DRUG*

István Horváth‡§, Veronika Harmat¶§, András Perczel‖, Villő Pálfi‖, László Nyitray,
Attila Nagy**, Emma Hlavanda‡, Gábor Náray-Szabó‡‡, and Judit Ovádi‡§§**

*From the ‡Institute of Enzymology, Biological Research Center, Hungarian Academy of Sciences, Karolina út 29
Budapest, H-1113 Hungary, ¶Protein Modeling Group, Hungarian Academy of Sciences, Eötvös Loránd University,
Pázmány sétány 1A, Budapest, H-1117 Hungary, ‖Department of Organic Chemistry, Eötvös Loránd University,
Pázmány sétány 1A, Budapest, H-1117 Hungary, and **Departments of Biochemistry and ‡‡Theoretical Chemistry,
Eötvös Loránd University, Pázmány sétány 1A, Budapest, H-1117 Hungary*

3′-(β-Chloroethyl)-2′,4′-dioxo-3,5′-spiro-oxazolidino-4-deacetoxyvinblastine (KAR-2) is a potent anti-microtubular agent that arrests mitosis in cancer cells without significant toxic side effects. In this study we demonstrate that in addition to targeting microtubules, KAR-2 also binds calmodulin, thereby countering the antagonistic effects of trifluoperazine. To determine the basis of both properties of KAR-2, the three-dimensional structure of its complex with Ca^{2+}-calmodulin has been characterized both in solution using NMR and when crystallized using x-ray diffraction. Heterocorrelation (^{1}H-^{15}N heteronuclear single quantum coherence) spectra of ^{15}N-labeled calmodulin indicate a global conformation change (closure) of the protein upon its binding to KAR-2. The crystal structure at 2.12-Å resolution reveals a more complete picture; KAR-2 binds to a novel structure created by amino acid residues of both the N- and C-terminal domains of calmodulin. Although first detected by x-ray diffraction of the crystallized ternary complex, this conformational change is consistent with its solution structure as characterized by NMR spectroscopy. It is noteworthy that a similar tertiary complex forms when calmodulin binds KAR-2 as when it binds trifluoperazine, even though the two ligands contact (for the most part) different amino acid residues. These observations explain the specificity of KAR-2 as an anti-microtubular agent; the drug interacts with a novel drug binding domain on calmodulin. Consequently, KAR-2 does not prevent calmodulin from binding most of its physiological targets.

Intracellular Ca^{2+} serves as a second messenger in response to external stimuli. The major Ca^{2+} receptor protein is calmodulin (CaM),[1] a ubiquitous, multifunctional protein that regulates at least 100 different proteins and enzymes. By assuming a new conformation upon binding that divalent cation, CaM transduces an elevation of intracellular Ca^{2+} levels to a change in enzyme activity (1). The three-dimensional structures of apo-CaM and Ca^{2+}·CaM have been determined by NMR and x-ray crystallography (3–8). CaM has similar N- and C-terminal lobes, within each of which are two Ca^{2+}-binding "EF-hand" motifs flanked by tightly structured domains (2). Upon binding Ca^{2+} ions, extensive hydrophobic surfaces become exposed to the solvent, promoting the interaction of CaM with target proteins. The CaM-binding domains of these target proteins are highly diverse in their amino acid sequences. One of the few unifying principles is the ability of all of these peptides to form basic, amphiphilic helices when complexed with Ca^{2+}·CaM (9). Three-dimensional structures of several ternary complexes of Ca^{2+}·CaM and a peptide from a target enzyme have been solved. In all of them, the two domains of CaM wraps around the peptide, contacting hydrophobic residues in the pocket between them (it also makes some polar interactions with surrounding acidic side chains) (10–12). The flexibility of the CaM molecule facilitates its binding to diverse peptides; both the backbone of its central region and its methyl methionine side chains extend toward the hydrophobic pockets that it forms. The degree of domain closure of CaM varies among these complexes. In recently published works; however, some target proteins are found to bind CaM in alternative ways (13). Certain target peptides assume only partially helical conformation, whereas others bind to just one domain of CaM or to dimerized CaM. In one structure, three helices of the target peptide bind an extended form of CaM (14–17).

Antagonists of CaM differ in both in their chemical structure and in their mechanism of action (18–20). Phenothiazines, arylalkylamines, naphtalenesulfonamides, calmidazolium, and felodipine are widely used in studying CaM functions. With a few exceptions (*e.g.* calmidazolium, compound 48/80, and AAA), such chemical antagonists bind to CaM with much lower affinity than do peptides (19, 21–24). (K_d in the micromolar and not nanomolar range, as described in Ref. 9 and references therein.) Using x-ray crystallography and NMR spectroscopy,

---

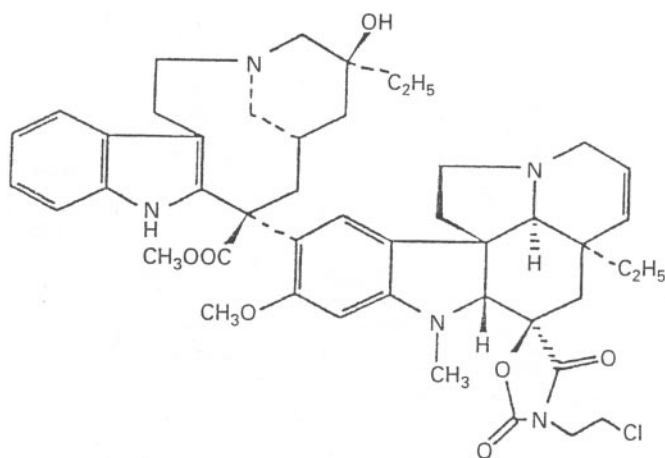**This paper is available on line at http://www.jbc.org**

FIG. 1. **Chemical structure of KAR-2.**

three-dimensional structures have been solved for complexes of CaM and such a competitive antagonists, *i.e.* with the phenothiazine TFP, with the naphthalenesulfonamide W7 (25), and with the arylalkylamine derivative AAA (26). The hydrophobic pockets of CaM are the primary binding sites for each of these three compounds.

Crystal structures are available for Ca^{2+}·CaM complexed with TFP in several stoichiometries (1:1, 1:2, and 1:4) (27–29). We have reported that in the case of the CaM·TFP_2 complex, the binding of the second TFP to an interdomain site can only occur following a conformational change induced by the binding of the first TFP molecule in the hydrophobic pocket of the C-terminal domain.

KARs are a series of semisynthetic bis-indol derivatives of vinblastine that block tubulin polymerization. Thereby they slow the growth of tumors yet exhibit lower toxicity to the host animal than does the parent compound (30). Following a screen of these compounds, we selected KAR-2 as the most effective antimitotic agent. The structure of KAR-2 is shown in Fig. 1, and its effect on cell viability, cell proliferation, and cell cycle in a neuroblastoma cell line (SH-SY5Y) has been described previously (31). At a concentration of the different compounds equivalent in causing 50% of inhibition of cell growth, KAR-2 induces complete arrest at the G_2/M transition, whereas vinblastine induced partial arrest in both G_0/G_1 and G_2/M. Moreover, the combination of KAR-2 and W13 (a naphthalenesulfonamide derivative with potent anti-CaM activity) arrests cancer cells both at the G_0/G_1 and the G_2/M transition, an effect resembling that of vinblastine. Levels of Cdc2 are much higher in KAR-2-treated cells than in those treated with vinblastine, indicating a stronger mitotic arrest. The effects of KAR-2 and vinblastine on the microtubular network have been analyzed by immunocytochemistry using anti-tubulin antibody (31). This deeper analysis of the two anti-cancer drugs reveals that KAR-2 causes the formation of aberrant mitotic spindles without effecting interphase microtubules, whereas vinblastine primarily damages the microtubule network of *interphase* cells.

We demonstrated previously that KAR-2 and vinblastine bind to CaM with comparable affinity (both in the micromolar range). Unlike vinblastine, however, KAR-2 does not abolish CaM's inhibition of phosphofructokinase (32) nor does it fully block the binding of a monospecific antibody to CaM (33). These data suggest that the complex of CaM with KAR-2 might have distinct structural and functional properties from that with vinblastine. In the present work, we use binding and functional tests to determine the effect of KAR-2 on CaM-related processes. In addition, we use x-ray crystallography to determine the three-dimensional structure of the protein-drug complex

and NMR spectroscopy to characterize the drug-binding site of the protein in solution. The resulting data contribute to an understanding of the role of CaM in cellular physiological, and they suggest what pharmacological intervention should be used to disrupt that function.

EXPERIMENTAL PROCEDURES

Proteins—CaM was purified from bovine brain using phenyl-Sepharose chromatography (34). For the NMR experiments, recombinant ^{15}N-labeled CaM was used. The plasmid vector encoding chicken gizzard CaM (cloned into pET-21d between the NcoI and BamHI sites) was a kind gift of Akio Nakamura (Gunma University, Japan). CaM was expressed in *Escherichia coli* BL21(DE3)pLysS cells. Uniform N^{15} labeling was achieved by growing 1 liter of culture with shaking at 37 °C in minimal medium containing 0.6% Na_2HPO_4, 0.3% KH_2PO_4, 0.05% NaCl, 0.4% glucose, 0.1% $^{15}NH_4Cl$ (Cambridge Isotope Labs), and ampicillin (50 μg/ml) until the absorbance at 600 nm reached 0.6. Protein expression was induced by the addition of 1 mM isopropyl 1-thio-β-D-galactopyranoside, and cultures were harvested 3 h later. Cells were then centrifuged (3 min at 4000 $\times$ g), washed with 100 ml of cold distillated water, and frozen at −80 °C. After thawing, cells were homogenized on ice by sonication (Sonifer 200, Branson, Danbury, CT) for 1 min. The supernatant from ultracentrifugation (100,000 $\times$ g for 60 min at 4 °C) was subjected to trichloreacetic acid precipitation of CaM. The recombinant CaM was further purified by column chromatography using 650 M butyl-Toyopearl (Tosoh, Tokyo, Japan). Remaining minor contaminants were removed by Sephacryl S-200 (Amersham Biosciences). Pooled fractions containing CaM were stored at −80 °C. Bovine brain CaM was biotinylated with biotin-XX-SSE (Molecular Probes, Eugene, OR, product code B-6352) as described previously (35).

Phosphodiesterase Assay—CaM-activated cAMP phosphodiesterase activity was assayed using an enzyme-coupled system according to Chock and Huang (36). The assay mixture contained 6 mM phosphoenolpyruvate, 0.3 mM ATP, 1.2 mM cAMP, 0.1 mM NADH, 0.01 units (4 nM) phosphodiesterase, 60 units myokinase, 11 units pyruvate kinase, 16 units lactate dehydrogenase, and 20 nM CaM in 66 mM Tris buffer containing 54 mM KCl, 0.03 mM $CaCl_2$, pH 7.5, at 30 °C. The reaction was started by addition of cAMP. All chemicals and enzymes used in the assay were purchased from Sigma.

Surface Plasmon Resonance—Surface plasmon resonance measurements were performed using a Biacore X instrument. The Sensor Chip SA (Biacore AB, Uppsala, Sweden, product code BR-1000–32) was activated with three consecutive injections of 20 μl of 1 M NaCl with 50 mM NaOH at a flow rate of 20 μl/min. 50 μg/ml biotinylated CaM was then injected over the streptavidin surface at 5 μl/min; the flow of the protein was stopped after the signal reached ~1000 response units. Two channels of the chip were used, one covered with CaM and the other was left blank and used as a control surface. In each experiment, 50 μl of aldolase at various concentrations and both with and without drugs was injected onto the surface at a flow rate of 10 μl/min. Both the association and dissociation phases were monitored for 300 s. The measured sensorgrams were fitted to Langmuir 1:1 curves using the BiaEvaluation 3.0 software, and the kinetic parameters of the interaction between CaM and aldolase were thereby inferred. All experiments were performed at 25 °C, and the eluent contained 50 mM HEPES, 150 mM KCl, 0.1 mM $CaCl_2$, and 0.005% surfactant P20 at pH 7.0. After each aldolase injection, the CaM surface was regenerated by injecting 20 mM EGTA for 300 s.

NMR Spectroscopy—^{15}N-^{1}H HSQC as well as 3-D HSQC-total correlation spectroscopy (mixing time 51.8 ms) and HSQC-nuclear Overhauser effect spectroscopy (mixing time 90 ms) spectra of ^{15}N-labeled CaM dissolved at a concentration of 1.2 mM in a 9:1 ratio of H_2O/D_2O containing 150 mM NaCl, 6.2 mM $CaCl_2$, and 0.01% NaN_3, pH 7.0, were recorded on a Bruker DRX 500 spectrometer at a temperature of 300 K. The spectrum of CaM alone was measured first, after which it was titrated by the stepwise addition of KAR-2 solution. A ratio of 1 part CaM to 1.5 parts KAR-2 was reached in five consecutive steps, thereby ensuring the saturation of CaM with that ligand. At each step in the titration, a complete ^{1}H-^{15}N HSQC spectrum was recorded. At the end of the titration, both total correlation spectroscopy and nuclear Overhauser effect spectroscopy spectra were measured. Partial resonance assignment was carried out using the two types of three-dimensional spectra; HSQC-total correlation spectroscopy spectra were measured to match amino acid residues with absorbance peak, whereas HSQC-nuclear Overhauser effect spectroscopy measurements were necessary to establish sequential connectivity between the identified spin systems (37, 38).

TABLE I
Data collection and refinement statistics of the calmodulin·KAR-2 crystal

Crystal parameters	
Space group	P6$_1$22
Cell constants	$a = b = 37.573$ Å, $c = 356.662$ Å
Data quality	
Resolution range (last resolution shell)	59.76–2.12 Å (2.20–2.12 Å)
R_{meas} [a]	0.074 (0.306)
Completeness	98.7% (88.7%)
No. of observed/unique	127375/9429 (8047/858)
$I/\sigma(I)$	23.39 (8.00)
Refinement residuals	
R	0.218
R_{free} [b]	0.261
Model quality	
Root mean square bond lengths (Å)	0.005
Root mean square bond angles (°)	1.215
Root mean square general planes (Å)	0.002
Ramachandran plot: residues in core/allowed/disallowed regions	120/7/0
Model contents	
Protein/KAR-2 residues	146/1
Protein atoms/KAR-2 atoms/Ca^{2+} ions/water molecules	2148/59/4/53
Residues in dual conformations	0
Residues with disordered side chains	12
Disordered residues	4

[a] $R_{meas} = (\Sigma_h(n/(n-1)))^{0.5} \Sigma_j|\langle I\rangle_h - I_{hj}|)/(\Sigma_{hj}I_{hj})$ with $\langle I_h\rangle = (\Sigma_j I_{hj})/n_j$.
[b] 4.8% of the reflections in a test set for monitoring the refinement process.

Circular Dichroism Spectroscopy—CD spectra were recorded with a JASCO J-720 spectropolarimeter. Measurements were made at 25 °C in 10 mM Tris, pH 7.0, in the presence of 200 μM CaCl$_2$ using a cuvette with a 1-cm path length. Spectra were recorded after a 5-min incubation of CaM with the drug(s), scanning each sample twice from 240–280 nm. In the case of three-part mixtures, the order of addition of ligands had no affect on the spectra. In the absence of CaM, no difference in the spectra was detected upon mixing vinblastine and TFP or KAR-2 and TFP. Spectral averaging and other mathematical operations were performed using the JASCO Standard Analysis software supplied by the instrument manufacturer.

Crystallization—Crystals of the CaM·KAR-2 complex were obtained using the hanging drop method by co-crystallization of 1 mM CaM and an equivalent amount of KAR-2 in 10 mM HEPES buffer, pH 7.00, containing 5 mM CaCl$_2$. The reservoir solution was 50 mM sodium cacodylate adjusted to pH 4.7 and containing 5 mM CaCl$_2$, 10 mM MgCl$_2$, and 26% (w/v) polyethylene glycol 8000. The drop contained a mixture of 2 μl of protein solution and 2 μl of reservoir solution.

The cryosolution contained 15% glycerol. Data were collected using the X11 beamline at the European Molecular Biology Laboratory Outstation at the Deutsches Elektronen-Synchrotron (DESY, Hamburg, Germany). A single crystal was rotated by 75° intervals (oscillation angle = 0.4°) and a consecutive 120° rotation interval (oscillation angle 0.1°). Data were processed with the XDS program package; they were scaled, merged, and reduced with XSCALE (39).

Determination and Refinement of X-ray Structure—The structure was solved by molecular replacement using the program MOLREP (40) of the Collaborative Computing Project 4 (41). The C-terminal domain of the CaM·TFP$_4$ complex (27) (Protein Data Bank (PDB) entry 1LIN) truncated to polyalanine was used as search model for both CaM domains. Refinement was carried out with the REFMAC5 program (42), using restrained maximum likelihood refinement and TLS refinement (43). ARP (44) was used for automatic solvent building. Model building was carried out using the O program (45). The final model contained residues 3–74 and 77–148, 4 calcium ions, 1 KAR-2 molecule, and 53 water molecules. The stereochemistry of the structure was assessed with PROCHECK (46). Data collection and refinement statistics are shown in Table I. The atomic coordinates and structure factors were deposited in the PDB with accession code 1XA5.

RESULTS AND DISCUSSION

Functional Studies—The potency of KAR-2 as an antagonist of calmodulin function is tested by the phosphodiesterase assay, a widely used method of measuring this property. When activated by Ca^{2+}·CaM, the enzyme phosphodiesterase hydrolyzes the second messenger molecule cAMP. Fig. 2*A* shows the inhibition of phosphodiesterase activity by several antagonists of calmodulin: KAR-2, its parent molecule vinblastine, and TFP. Calmodulin-dependent phosphodiesterase activity is com-

pletely eliminated by sufficient concentrations of TFP and vinblastine (IC$_{50}$ of 13.4 $\pm$ 4.9 μM and 188.4 $\pm$ 78.6 μM, respectively). KAR-2, by contrast, never decreases calmodulin-dependent phosphodiesterase activity below ~50% of the starting level. (This degree of inhibition is achieved at a drug concentration of 20 μM.) In summary, the three drugs have dramatically different effects on such phosphodiesterase activity despite exhibiting similar affinities for CaM. We propose that KAR-2 interacts with a different binding domain of CaM from that targeted by TFP and vinblastine.

To test this hypothesis, we measured CaM-activated phosphodiesterase activity in the presence of saturating concentrations of both TFP and KAR-2. The data in Fig. 2*B* show that the presence of KAR-2 reduces the inhibitory effect of TFP even at concentrations that would completely inhibit calmodulin-dependent phosphodiesterase activity in the absence of the former compound. In fact, in the presence of high concentrations of both drugs, phosphodiesterase activity is ~50% of that observed with neither. In other words, calmodulin-dependent phosphodiesterase activity at saturating levels of KAR-2 is essentially independent of the concentration of TFP. We conclude that KAR-2 functions as a "liberator" of inactivated calmodulin, counteracting the antagonist effect of TFP.

Binding Studies—Surface plasmon resonance experiments are carried out to characterize the effects of KAR-2 and other drugs on the interaction of CaM with target enzymes. To this end, biotinylated CaM is immobilized on a streptavidin-covered chip. This system is exposed to a mobile phase that contains aldolase as a target protein. The rational for using aldolase instead of phosphodiesterase in surface plasmon resonance measurements is that CaM has comparable binding affinities for aldolase as for the drugs used in this study. Consequently, meaningful data can be obtained using comparable concentrations of aldolase and drugs. Several successive experiments use the same calmodulin-coated chip that has been regenerated by washing with 20 mM EGTA. Fig. 3*A* shows the sensorgrams of aldolase binding measured at different concentrations of aldolase. Rate constants for association and dissociation and the equilibrium dissociation constant are inferred from these curves: $k_a = (617.0 \pm 2.73)$ M^{-1} s^{-1}, $k_d = (1.95*10^{-4} \pm 1.86*10^{-5})$ s^{-1}, and $K_d = k_d/k_a = 3.16*10^{-7}$ M.

These values are in good agreement with data obtained previously by Orosz *et al.* (47). The inset in Fig. 3*A* illustrates that

A

B

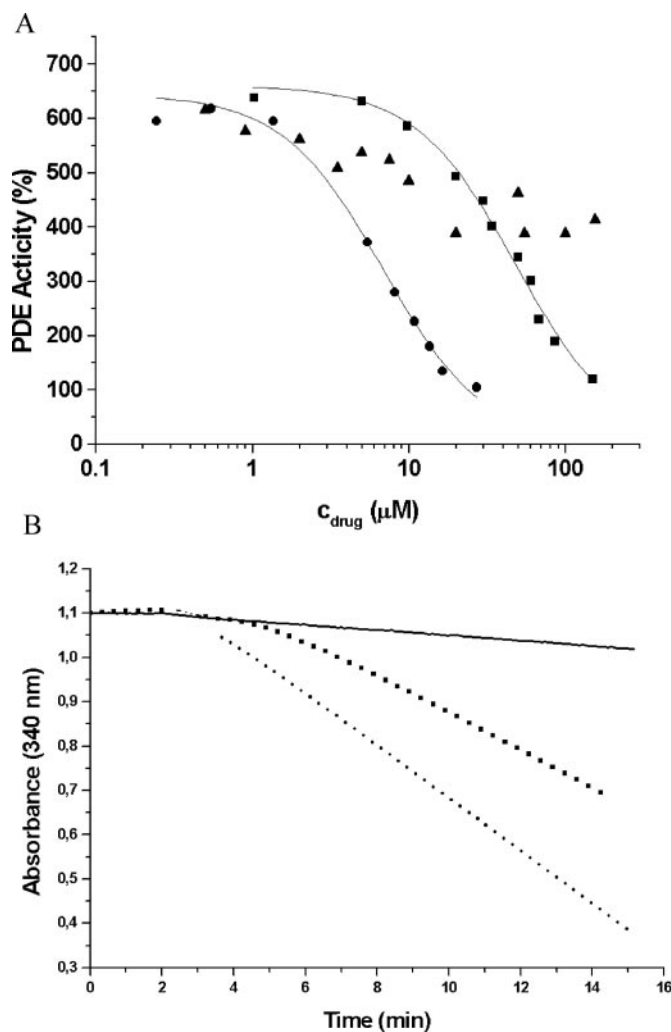FIG. 2. **The anti-CaM potencies of drugs tested by CaM-activated phosphodiesterase (*PDE*) assay.** *A*, displacement curves for TFP (●), vinblastine (■), and KAR-2 (▲). 100% PDE activity corresponds to the reaction rate measured without CaM. *B*, liberator effect of KAR-2. The rate of cAMP hydrolysis was followed spectrophotometrically at 340 nm in the presence of 27.3 μM TFP (*solid line*), 27.3 μM TFP + 37.5 μM KAR-2 (*dashed line*), and without drugs (*dotted line*). For other details see "Experimental Procedures."

the R_{eq} value (a measure of the quantity of the protein·protein complex) is directly proportional to the aldolase concentration. These control measurements demonstrate that 5 μM aldolase is an appropriate concentration for injected drugs to produce detectable perturbation of the system. According to our expectations, 20 μM TFP prevents the binding of aldolase to immobilized CaM. By contrast, KAR-2 only partially inhibits the association of aldolase with CaM (never more than 40% inhibition as shown in Fig. 3, *B* and *C*). These observations are consistent with earlier studies using fluorescence anisotropy in which we showed that KAR-2 only partially inhibits the formation of a CaM-phosphofructokinase complex (32).

In conclusion, these findings on protein association agree with those of the functional studies illustrated in Fig. 2; both observations are explained by positing that KAR-2 and TFP target different domains of CaM. In the one case, the KAR-2·CaM·enzyme ternary complex retains a conformation in which CaM partially activates the bound enzyme. By contrast, TFP·CaM binary complex cannot bind to the target enzyme because TFP and the enzyme compete for CaM binding. The former case resembles CaM complexed with the arylalkylamine

derivative KHL-8430 and the target enzyme; however, CaM loses its activating effect in that situation (48).

Structural Studies—To determine the structural basis of the remarkable functional properties of KAR-2, we decided to solve the structure of the CaM·KAR-2 complex both in crystals and in solution. Crystals of this complex are obtained by co-crystallizing KAR-2 and CaM, using conditions similar to those that produce CaM·TFP$_2$ crystals (Ref. 29 and "Experimental Procedures"). The resulting structure of the CaM·KAR-2 complex is well defined by the electron density map except for residues Ala-1, Asp-2, Lys-75, Met-76 and the side chains of residues Lys-77, Asp-78, Asp-80, Lys-94, Leu-105, Arg-106, Lys-115, Glu-119, Glu-123, Arg-126, Ile-130, and Glu-139. The protein is in a closed compact conformation. The bound KAR-2 molecule is also well defined by its electron density map, being situated in an interdomain position between the N- and C-terminal lobes of CaM (Fig. 4, *A* and *B*). The compact conformation of CaM induced upon binding KAR-2 resembles that assumed by CaM when it is bound by TFP molecule or by most cognate peptides (10–12, 27–29). Overlaying the CaM·KAR-2 and CaM·TFP$_1$ structures (Fig. 4*A*) clearly demonstrates that KAR-2 and the C-terminal-bound TFP are accommodated in distinct sites on CaM. Indeed, most of the amino acid residues contacted by the respective drugs are different. The catharantine region of KAR-2 principally contacts hydrophobic residues (Phe-19, Leu-39, Phe-68, Met-71, Met-72) of the N-terminal domain of CaM (Fig. 4*B*). The indole moiety of the drug is bound in a shallow depression on the surface of CaM. This depression is also found in some CaM·peptide complexes accommodating a hydrophobic side chain of the target (most enhanced in complexes with the rat Ca^{2+}·CaM-dependent protein kinase and CaM-dependent kinase II) (12, 49). Most of the contacts of the vindoline moiety (which contains the oxazilidino ring characteristic of this bis-indol derivative) are formed with residues in the C-terminal lobe of CaM. In contrast to the catharantine region, however, this part of the drug does not exclusively contact hydrophobic side chains (Ile-85, Met-109, Met-124, Met-144, Met-145). It also makes several important interactions with polar residues (Glu-84, Glu-114, Lys-148). The polarizable chlorine atom of KAR-2 contacts the Sδ atom of Met-109 and the carboxylate group of Glu-114 (Fig. 4*B*).

A surprising feature of the interface between KAR-2 and CaM is that the two hydrophobic pockets are missing from the protein because of intradomain motions. In fact, this conformational change has removed the primary target of most cognate peptides and many drugs. KAR-2 is accommodated by a novel conformation of CaM, assumed upon subtle shifts in ϕ-ψ angles that reposition the helices (Fig. 4, *C* and *D*). Slight closure of the IV and VII helices, respectively, causes the side chains of Met-71 and Met-144 to occlude the hydrophobic cavities of the N- and C-terminal lobes. The only precedent for this effect is the CaM·myristoylated alanine-rich C kinase substrate peptide complex (PDB accession code 1IWQ) (50) in which a small change of the angle between helices III and IV causes narrowing of the hydrophobic pocket in the N-terminal domain. The above phenomenon suggests that in the CaM·KAR-2·TFP complex the conformation of CaM does not allow binding of TFP the usual way (27–29) to the hydrophobic pocket of the C-terminal domain.

Comparing many structures of CaM in complex with a drug or peptide, one finds that all ligands principally contact a single face within each protein domain. This common feature aside, however, the known structures of calmodulin interacting with ligands are remarkably diverse. Some structures have CaM in an extended conformation; others show ligand bound to one protein domain whereas the other is empty, and yet others
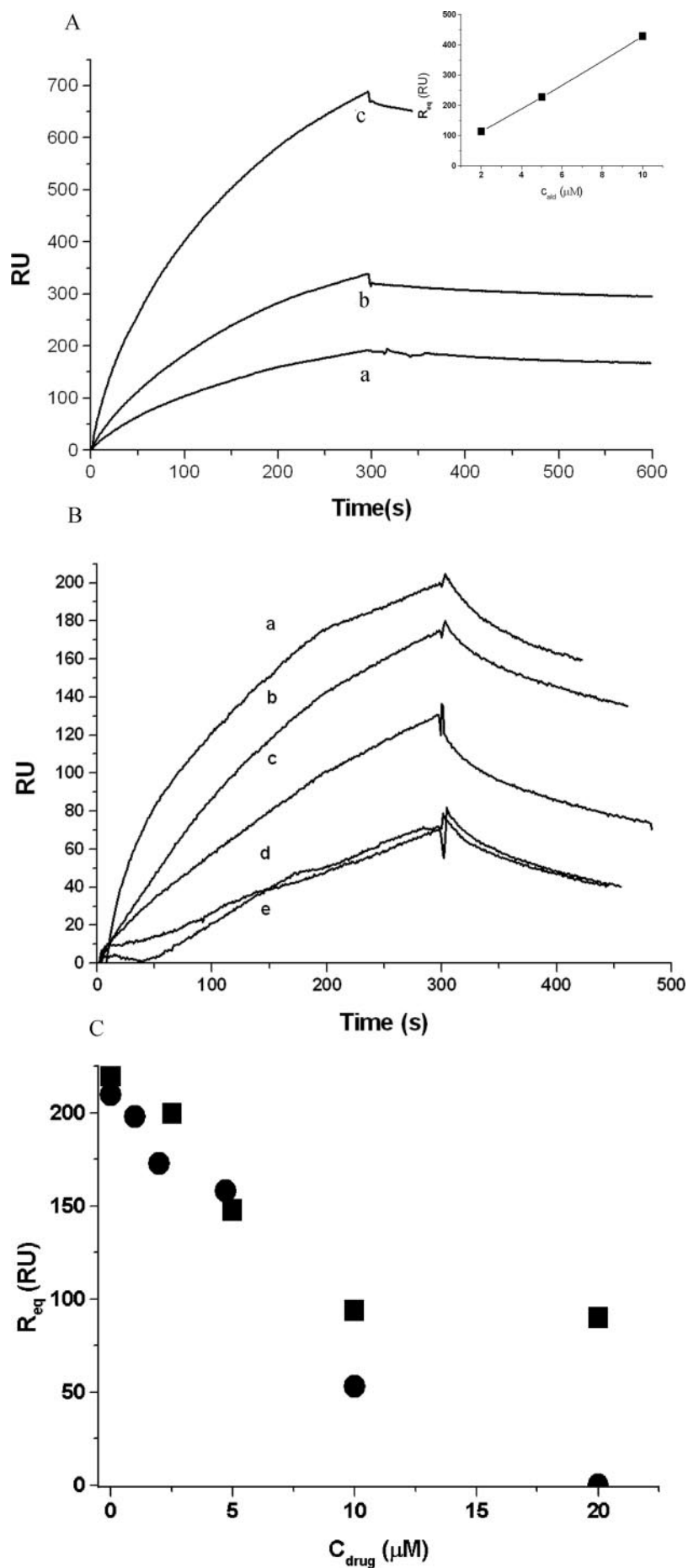
FIG. 3. **Surface plasmon resonance measurements.** *A*, binding of aldolase to the CaM. Aldolase was injected onto the CaM covered surface in various concentrations: 2 μM (*solid line*), 5 μM (*dotted line*), and 10 μM (*dashed line*). The *inset* shows the calculated R_{eq} values for each aldolase concentration. *B*, effect of KAR-2 on aldolase binding to CaM. 5 μM enzyme was injected together with 0 (*a*), 2.5 μM (*b*), 5 μM (*c*), 10 μM (*d*), and 20 μM (*e*) KAR-2. *C*, dependence of RU_{eq} (where *RU* is response unit) on KAR-2 (*squares*) and TFP (*circles*) concentrations.
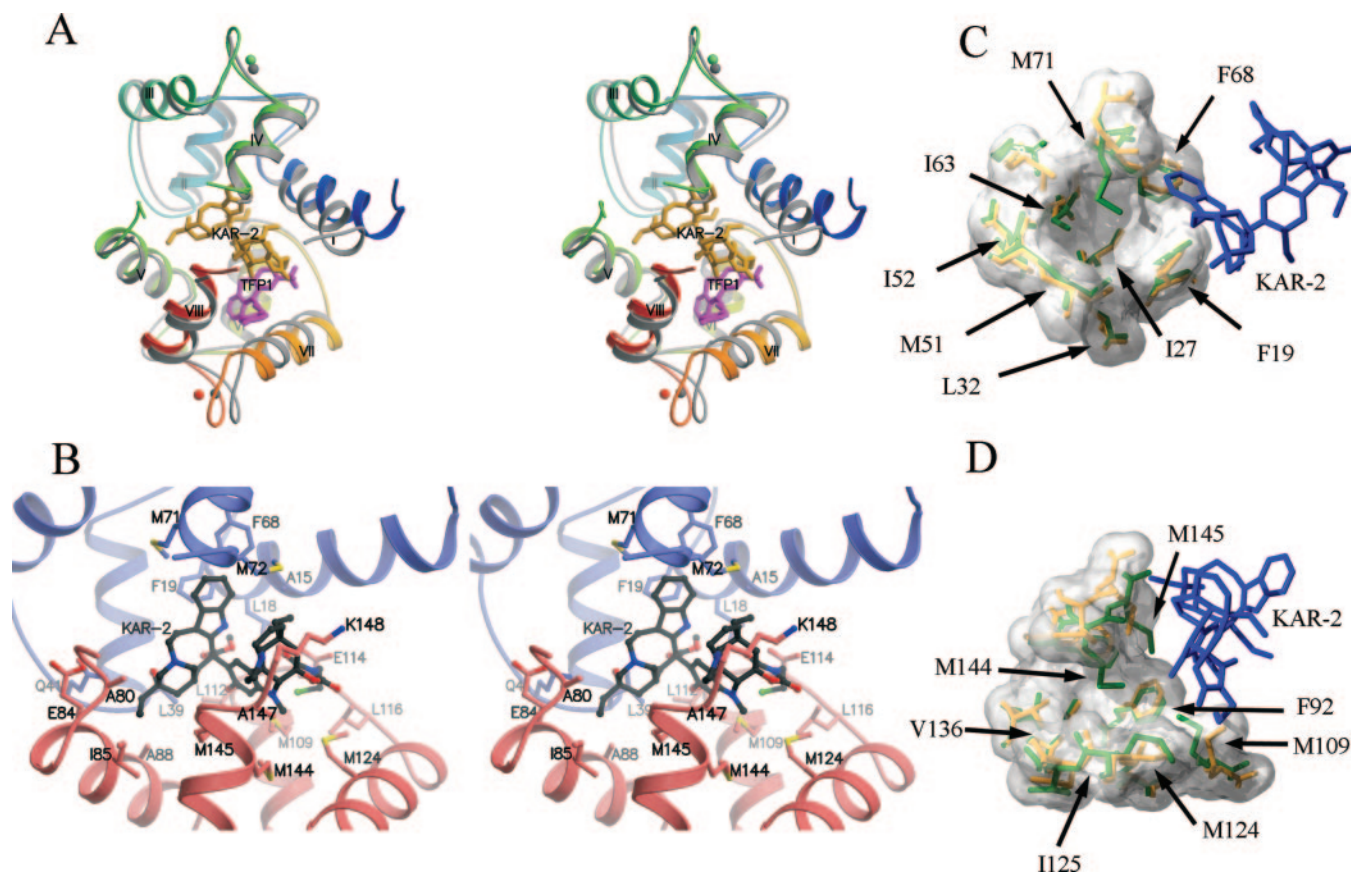
FIG. 4. *A*, stereo view of the superimposition of CaM·KAR-2 (from *blue* to *red*) and CaM·TFP (*gray*) (PDB accession code 1CTR) structures. KAR-2 (*yellow*) and TFP (*purple*) bind to different sites on CaM. Although the global conformation is similar, TFP binds to the hydrophobic pocket at the C-terminal domain, whereas KAR-2 is bound between the two domains. *B*, a closer view of the binding site; side chains contacting KAR-2 (atom-atom distances shorter than 4.2 Å) are shown. KAR-2 interacts with residues both from the N-terminal (*blue*) and C-terminal (*rose*) domains. *C* and *D* show the hydrophobic pockets of the N-terminal and C-terminal domains, respectively. The CaM·KAR-2 complex (*green*) is superimposed on the Ca^{2+}·CaM structure (PDB accession code 1CLL, *yellow*, molecular surface calculated for 1CLL is shown in *gray*). Hydrophobic pockets of both the N- and C-terminal domains are masked by methionine residues (Met-71, Met-109, Met-144, and Met-145) as a result of KAR-2 binding. *A* and *B* were created with MolScript 2.1 (52) and rendered by Raster3D (53). For *C* and *D* SwissPDBViewer 3.7 (54) was used to create the scenes, and the rendering was done by POW-ray 3.5.

include more than one peptide chain bound between the domains of CaM. In light of this variability, we speculate that the ternary complex of enzyme·CaM·KAR-2 differs from the binary one of CaM·KAR-2; the conformation of CaM is much less closed in the former structure. The eight-membered ring of KAR-2 is not rigid and can change conformation even when the drug is bound to CaM. Consequently, the protein portion of the CaM·KAR-2 complex can also adapt its conformation to best fit the target enzyme.

NMR Studies—Multiple NMR experiments have been performed on CaM bound by KAR-2, thereby determining whether the crystal structure truly resembles that of the complex in solution. In these procedures, ^{15}N-labeled CaM is titrated with KAR-2. Superposing the ^{1}H-^{15}N HSQC spectra recorded at increasing concentrations of that ligand, we discover significant peak displacements (Fig. 5). Among the peaks that have been assigned to specific residues, 20 show significant changes in their chemical shift (Fig. 6). Half of these represent residues in the N-terminal lobe of CaM, and the other half correspond to residues in the C-terminal domain. These data on the drug·protein complex in solution are consistent with the structure determined by x-ray crystallography; both lobes of CaM are involved in KAR-2 binding. The aforementioned changes of chemical shifts are caused either by the interaction of target amino acid residues with KAR-2 or by the domain closure of CaM and the emerging interface between its two domains.

To distinguish between these two effects and to interpret the

heterocorrelation NMR data, we make further comparisons between the data gathered by NMR spectroscopy and that obtained using x-ray crystallography. In the x-ray structure, we note two contact regions that form between the N- and C-terminal domains of CaM upon formation of the complex with KAR-2. (Such interactions between domains of CaM are in addition to those of CaM with KAR-2 that are shown in Fig. 6.) To be precise, we note contacts that form between helix I in the N-terminal domain and the loop between helices VI and VII in the C-terminal domain and between helix V (C-terminal domain) and the loop between helices II and III (N-terminal domain). We believe that these new contacts between the two lobes of CaM may be responsible for many of the observed changes in chemical shift values. By contrast, we attribute to direct contact with KAR-2 those changes in the chemical shifts of peaks representing Ala-15, Phe-16, and Leu-18. (These changes of chemical shift could also be attributed to novel interaction between helices I and VII upon the binding of CaM to KAR-2.) Either explanation is consistent with the crystal structure of the CaM·KAR-2 complex (Fig. 6), because Ala-15 and Phe-19 are in close proximity to KAR-2 and also to Glu-14, Leu-18, Leu-112, and Glu-114. Furthermore, the changes of chemical shift for peaks corresponding to Leu-39 and Gly-40 are in good agreement with structural changes revealed by x-ray crystallography. Leu-39 is apt to contact KAR-2, whereas Gly-40, Gln-41, and Asn-42 (residues forming a loop connecting helices II and III) move because of an interaction with Glu-84
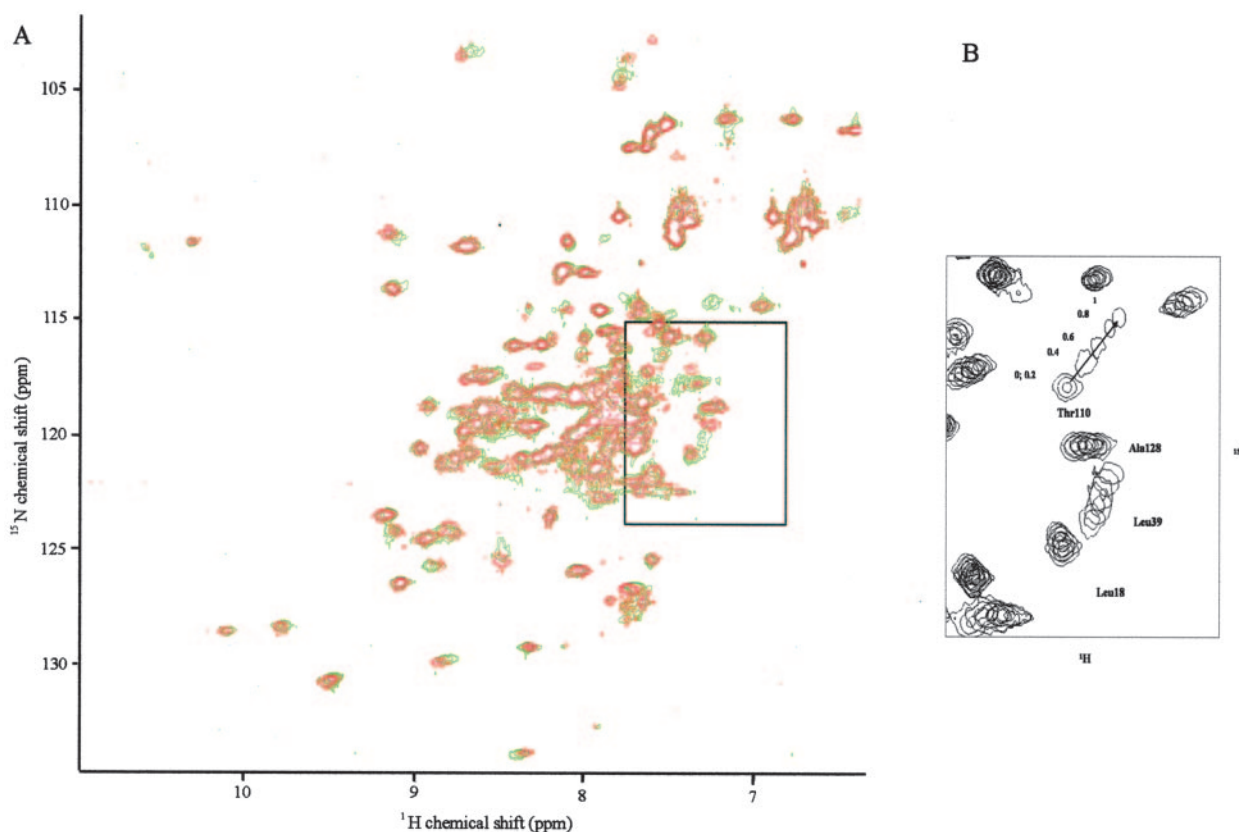
FIG. 5. *A*, ^{1}H-^{15}N HSQC spectra of 1 mM [^{15}N]CaM; chemical shift changes of CaM upon KAR-2 addition in the absence (*red*) and presence (*green*) of an equivalent amount of KAR-2. Vertical axis is the ^{15}N shift; the horizontal axis is the ^{1}H shift in ppm. *B*, some assigned peaks of an enlarged part of the spectra. The numbers next to the Thr-110 peaks indicate the KAR-2/CaM ratio.
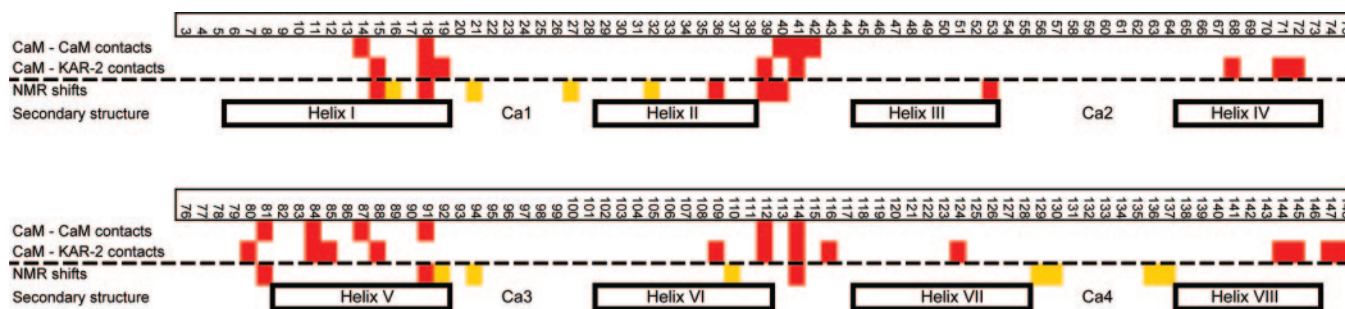

FIG. 6. **Comparison of the structural data obtained by x-ray diffraction and NMR spectroscopy.** *First lane*, *red boxes* along the CaM sequence show residues involved in the formation of CaM-CaM interdomain contacts by binding of KAR-2 ($d \leq 4.2$ Å, comparison of the crystal structure of CaM·KAR-2 and Ca^{2+}·CaM with PDB accession code 1CLL). *Second lane*, residues of CaM contacting KAR-2 in the crystal structure are labeled with *red boxes*. *Third lane*, the effect of KAR-2 binding on amide NH chemical shifts of CaM. Residues involved in major and minor chemical shift changes are labeled with *red* or *yellow boxes*, respectively. Secondary structure elements of CaM are shown in the *fourth lane*. Some of the chemical shift changes are attributed to interactions detected in the crystal structure of CaM·KAR-2. This suggests the closed compact structure of CaM·KAR-2 obtained by x-ray diffraction is also dominant in solution.

and Glu-87 of helix V. The chemical shift of the peak corresponding to Ser-81 undergoes a major change, most likely on account of a novel interaction between helices III and V. (In the x-ray structure, this conformational change is greatest for Ser-81, Glu-84, and Glu-87, all of which are located on one side of helix V.) The large NMR shift of the peak corresponding to Val-91 and the somewhat smaller ones corresponding to the peaks for Phe-92 and Lys-94 are almost certainly caused by rearrangement of the CaM lobes induced by its binding the KAR-2 ligand. Finally, the very noticeable change of the chemical shift for Glu-114 may either come from the interaction of helices I and VI or from a direct contact between that residue and KAR-2.

In summary, by comparing the crystallographic and NMR data we are able to interpret most of the shifts observed. As is

observed independently by crystallography, our NMR results show that the CaM·KAR-2 complex is in a "closed" conformation. In solution, as in the crystal, binding of the KAR-2 ligand induces novel contacts between surfaces of the N- and C-terminal domains of CaM.

CD Spectroscopy—In the absence of a crystal structure for the CaM·vinblastine complex, we use CD spectropolarimetry to get circumstantial evidence for distinct binding sites of KAR-2 and vinblastine on CaM. In an earlier application of CD spectropolarimetry, we demonstrate sequential binding of two TFP molecules to CaM (29). The binding of the first TFP molecule to the hydrophobic pocket of the C-terminal domain is detected as a negative difference CD peak at 263 nm. The subsequent appearance of a positive peak at 270 nm corresponds to the interaction of the second TFP molecule with an interdomain

FIG. 7. **Distinct effects of KAR-2 and vinblastine on the formation of CaM·TFP complexes.** *A*, difference spectra of 10 μM CaM with 30 μM TFP without (*solid line*) and with 30 μM KAR-2 (*dotted line*). *B*, difference spectra of 10 μM CaM and 10 μM TFP without (*solid line*) and with 10 μM vinblastine (*dotted line*). For other details see "Experimental Procedures."
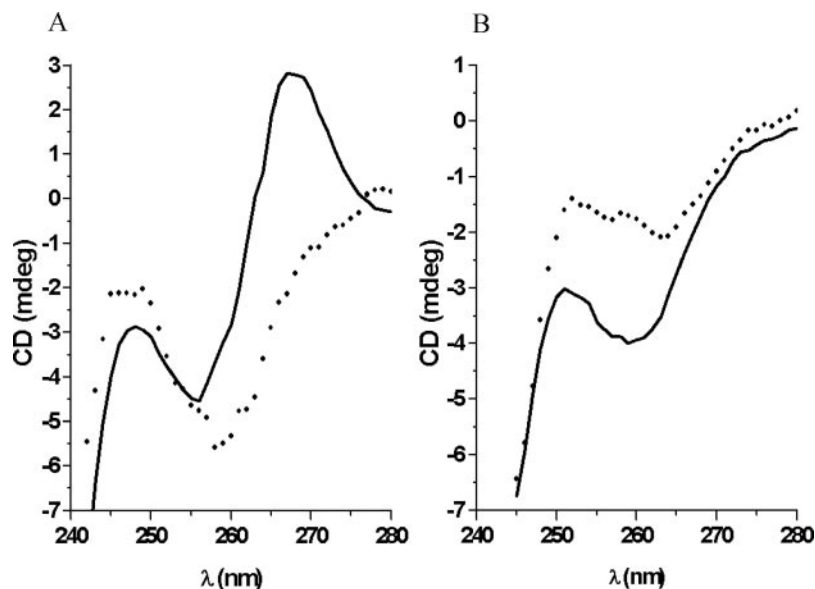
site on CaM (Fig. 7*A*). The addition of a stoichiometric amount of KAR-2 to the CaM·TFP$_1$ complex does not perturb the CD spectrum (data not shown). By contrast, addition of a KAR-2 to the CaM·TFP$_2$ complex eliminates the positive peak corresponding to the second bound TFP (*cf.* Fig. 7). This observation is explained by our crystallographic data (*cf.* Fig. 4); KAR-2 is bound in an interdomain site on CaM. In contrast to the situation with KAR-2, the addition of 1 equivalent of vinblastine to CaM·TFP$_1$ complex significantly reduced the negative peak. This stoichiometry reflects the binding of TFP to the hydrophobic pocket of the C-terminal domain. We draw two conclusions: 1) the binding of vinblastine to CaM counters that of the first TFP, and 2) although they are both derivatives of bis-indol, KAR-2 and vinblastine bind to different sites on CaM. Knowing the crystal structure of the CaM·KAR-2 complex, it is possible to interpret these changes in the CD spectra as distinct interactions of CaM with vinblastine and KAR-2.

Structure and Function Relationship and Beyond—The major objectives of this work are to elucidate the effects of KAR-2 on the structure of calmodulin and to determine the effects of that potent anti-mitotic agent on the physiological activity of the calcium-binding protein. To these ends, we determine the three-dimensional structure of the CaM·KAR-2 complex and characterize the effect of KAR-2 on the interaction of CaM with a target enzyme (aldolase). The project is motivated by the unique properties of KAR-2 as an anti-cancer agent in cells and animals (31, 51). We believe that our studies of *in vitro* systems resolve the following paradox arising from *in vivo* investigations. Vinblastine is toxic in much lower concentration than KAR-2 both to cultured cells and to test animals. This difference in the index of toxicity between vinblastine and KAR-2 is observed despite their similar anti-microtubular activities and comparable affinities for the vinca site of tubulin (31). Our explanation is that vinblastine is a potent CaM antagonist, whereas KAR-2 is a rather ineffective one. The toxicity of vinblastine can be attributed (at least in large part) to its impact on CaM-related physiological processes. Perturbation of CaM-driven processes that regulate the cell cycle are expected to have toxic side effects much like those observed during chemotherapy with vinblastine.

Our central observation is that KAR-2 and vinblastine exert similar effects on tubulin/MT-related assays but a distinct effect on CaM-related assays. We find that vinblastine affects CaM as does TFP, a competitive antagonist that binds to the hydrophobic pocket of the C-terminal domain of CaM. Accord-
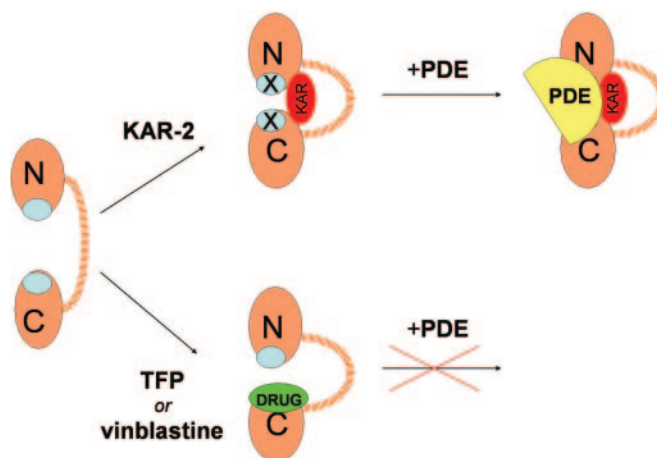

FIG. 8. **Distinct binding sites of KAR-2 and TFP on CaM and distinct effects on activity of CaM-activated phosphodiesterase (PDE).** *N* and *C* denote the domains of CaM; hydrophobic pockets are *blue*. In the case of KAR-2 a ternary complex is formed allowing CaM to activate the enzyme, whereas TFP and vinblastine inhibit the formation of CaM·target protein complex.

ing to our CD measurements, vinblastine competes with the first TFP molecule to bind to the CaM protein. For this reason, we suspect that vinblastine is accommodated in the hydrophobic pocket of the C-terminal domain, that part of CaM responsible for binding and activating target enzymes. (Confirmation of this model must await solution of a three-dimensional structure of the CaM-vinblastine complex.) KAR-2, however, does not fit into this pocket, leaving it to interact with an interdomain region of CaM.

Our present crystallographic and NMR data provide direct evidence for the site on CaM that binds KAR-2. Overlaying the structures of CaM·KAR-2 and CaM·TFP$_1$ (Fig. 4*A*), it is clear that KAR-2 and TFP (the molecule bound to the C-terminal domain of CaM) are accommodated in distinct sites. Indeed, few amino acid residues of CaM are observed to contact both drugs. KAR-2 induces/stabilizes a closed conformation of CaM, occluding the tunnel between the two domains and reorienting the two domains so as to alter their hydrophobic pockets (Fig. 4, *C* and *D*). Even when complexed with KAR-2, CaM can still bind TFP, explaining the "non-competitive" and "non-antagonist" behavior of KAR-2. Unlike the situation with TFP and vinblastine, we find that KAR-2 never fully blocks CaM from

activating phosphodiesterase or phosphofructokinase (Fig. 8). In future work, we will attempt to identify those CaM-modulated processes that are inhibited by vinblastine but not by KAR-2, as they are apt to cause the unpleasant side effects of the former drug.

REFERENCES

1. Klee, C. B., and Vanaman, T. C. (1982) in *Advances in Protein Chemistry* (Anfinsen, C. B., Edsall, J. T., and Richards, F. M., eds) Vol. 35, pp. 213–321, Academic Press, New York
2. Nakayama, S., and Kretsinger, R. (1994) *Annu. Rev. Biophys. Biomol. Struct.* **23,** 473–507
3. Zhang, M., Tanaka, T., and Ikura, M. (1995) *Nat. Struct. Biol.* **2,** 758–767
4. Kuboniwa, H., Tjandra, N., Grzesiek, S., Ren, H., Klee, C. B., and Bax, A. (1995) *Nat. Struct. Biol.* **2,** 768–776
5. Finn, B. E., Evenäs, J., Drakenberg, T., Waltho, J. P., Thulin, E., and Forsén, S. (1995) *Nat. Struct. Biol.* **2,** 777–783
6. Babu, Y. S., Sack, J. S., Greenhough, T. J., Bugg, C. E., Means, A. R., and Cook, W. J. (1985) *Nature* **315,** 37–40
7. Kretsinger, R., Rudnick, S., and Weissman, L. (1986) *J. Inorg. Biochem.* **28,** 289–302
8. Fallon, J. F., and Quiocho, F. A. (2003) *Structure* (*Lond.*) **11,** 1303–1307
9. O'Neil, K. T., and DeGrado, W. F. (1990) *Trends Biochem. Sci.* **15,** 59–64
10. Ikura, M., Clore, G. M., Gronenborn, A. M., Zhu, G., Klee, C. B., and Bax, A. (1992) *Science* **256,** 632–638
11. Meador, W. E., Means, A. R., and Quiocho, F. A. (1992) *Science* **257,** 1251–1255
12. Meador, W. E., Means, A. R., and Quiocho, F. A. (1993) *Science* **262,** 1718–1721
13. Vetter, S. W., Leclerc, E. (2003) *Eur. J. Biochem.* **270,** 404–414
14. Drum, C. L., Yan, S. Z., Bard, J., Shen, Y. Q., Lu, D., Soelaiman, S., Grabarek, Z., Bohm, A., and Tang, W. J. (2002) *Nature* **415,** 484–489
15. Elshorst, B., Hennig, M., Försterling, H., Diener, A., Maurer, M., Schulte, P., Schwalbe, H., Griesinger, C., Krebs, J., Schmid, H., Vorherr, T., and Carafoli, E. (1999) *Biochemistry* **38,** 12320–12332
16. Schumacher, M. A., Rivard, A. F., Bachinger, H. P., and Adelman, J. P. (2001) *Nature* **410,** 1120–1124
17. Kurokawa, H., Osawa, M., Kurihara, H., Katayama, N., Tokumitsu, H., Swindells, M. B., Kainosho, M., and Ikura, M. (2001) *J. Mol. Biol.* **312,** 59–68
18. Hait, W. N., and Lazo, J. S. (1986) *J. Clin. Oncol.* **4,** 994–1012
19. Johnson, J. D., and Mills, J. S. (1986) *Med. Res. Rev.* **6,** 341–363
20. Linse, S., Drakenberg, T., and Forsen, S. (1986) *FEBS Lett.* **199,** 28–32
21. Sobieszek, A. (1989) *Biochem. J.* **262,** 215–223
22. Orosz, F., Christova, T. Y., and Ovádi, J. (1988) *Mol. Pharmacol.* **33,** 678–682
23. Tanaka, T., Hidaka, H. (1980) *J. Biol. Chem.* **255,** 11078–11080
24. Gietzen, K. Adamczyk-Engelmann, P., Wuthrich, A., Konstantinova, A., and Bader, H. (1983) *Biochim. Biophys. Acta* **736,** 109–118
25. Osawa, M., Swindells, M. B., Tanikawa, J., Tanaka, T., Mase, T., Furuya, T., and Ikura, M. (1998) *J. Mol. Biol.* **276,** 165–176
26. Harmat, V., Böcskei, Z., Náray-Szabó, G., Bata, I., Csutor, A. S., Hermecz, I., Arányi, P., Szabó, B., Liliom, K., Vértessy, B. G., and Ovádi, J. (2000) *J. Mol. Biol.* **297,** 747–755
27. Vandonselaar, M., Hickie, R. A., Quail, J. W., and Delbaere, L. T. J. (1994) *Nature Struct. Biol.* **1,** 795–801
28. Cook, W. J., Walter, L. J., and Walter, M. R. (1994) *Biochemistry* **33,** 15259–15265
29. Vértessy, B. G., Harmat, V., Böcskei, Z., Náray-Szabó, G., Orosz, F., and Ovádi, J. (1998) *Biochemistry* **37,** 15300–15310
30. Orosz, F., Kovács, J., Lőw, P., Vértessy, B. G., Urbányi, Z., Ács, T., Keve, T., and Ovádi, J. (1997) *Br. J. Pharmacol.* **21,** 947–954
31. Comin-Anduix, B., Agell, N., Bachs, O., Ovadi, J., and Cascante, M. (2001) *Mol. Pharmacol.* **60,** 1235–1242
32. Orosz, F., Vértessy, B. G., Salerno, C., Crifo, C., Capuozzo, E., and Ovádi, J. (1997) *Br. J. Pharmacol.* **21,** 955–962
33. Molnár, A., Liliom, K., Orosz, F., Vértessy, B. G., and Ovádi, J. (1995) *Eur. J. Pharmacol.* **291,** 73–82
34. Gopalakrishna, R., and Anderson, W. B. (1982) *Biochem. Biophys. Res. Commun.* **104,** 830–836
35. Kincaid, R. L., Billingsley, M. L., and Vaughan, M., (1988) *Methods Enzymol.* **159,** 605–626
36. Chock, S., and Huang, C. Y. (1984) *Anal. Biochem.* **138,** 34–43
37. Talluri, S., and Wagner, G. (1996) *J. Magn. Reson. B* **112,** 200–205
38. Mori, S., Abeygunawardana, C., Johnson, M. O., and van Zilj, P. C. (1995) *J. Magn. Reson. B* **108,** 94–98
39. Kabsch, W. (1993) *J. Appl. Crystallogr.* **26,** 795–800
40. Vagin, A., and Teplyakov, A. (2000) *Acta Crystallogr. Sect. D Biol. Crystallogr.* **56,** 1622–1624
41. Collaborative Computational Project 4 (1994) *Acta Crystallogr. Sect. D Biol. Crystallogr.* **50,** 760–763
42. Murshudov, G. N., Vagin, A. A., and Dodson, E. J. (1997) *Acta Crystallogr. Sect. D Biol. Crystallogr.* **53,** 240–255
43. Winn, M. D., Isupov, M. N., and Murshudov, G. N. (2001) *Acta Crystallogr. Sect. D Biol. Crystallogr.* **57,** 122–133
44. Lamzin, V. S., and Wilson, K. S., (1997) *Methods Enzymol.* **277,** 269–305
45. Jones, T. A., Zou, J. Y., Cowan, S. W., and Kjeldgaard, M. I. (1991) *Acta Crystallogr. Sect. A* **47,** 110–119
46. Laskowski, R. A., MacArthur, M. W., Moss, D. S., and Thornton, J. M. (1993) *J. Appl. Crystallogr.* **26,** 283–291
47. Orosz, F., Christova, T. Y., and Ovádi, J. (1988) *Biochim. Biophys. Acta* **957,** 293–300
48. Orosz, F., Telegdi, M., Liliom, K., Solti, M., Korbonits, D., and Ovádi, J. (1990) *Mol. Pharmacol.* **38,** 910–916
49. Wall, M., Clarage, J. B., and Phillips, G. N. (1997) *Structure* (*Lond.*) **5,** 1599–1612
50. Yamauchi, E., Nakatsu, T., Matsubara, M., Kato, H., and Taniguchi, H. (2003) *Nat. Struct. Biol.* **10,** 226–231
51. Orosz, F., Comin, B., Rais, B., Puigjaner, J., Cascante, M., Kovács, J., Tárkányi, G., Ács, T., Keve, T., and Ovádi, J. (1999) *Br. J. Cancer* **79,** 1356–1365
52. Kraulis, P. J. (1991) *J. Appl. Crystallogr.* **24,** 946–950
53. Merritt, E., and Bacon, D. J. (1997) *Methods Enzymol.* **277,** 505–524
54. Guex, N., and Peitsch, M. C. (1997) *Electrophoresis* **18,** 2714–2723